Journal of Marine Systems 241 (2024) 103909

Contents lists available at ScienceDirect

Journal of Marine Systems

journal homepage: www.elsevier.com/locate/jmarsys

Wind-driven advection across temperature gradients enhances iron-induced phytoplankton blooms in the Antarctic Polar Front

F.P. Brandini [a,*], A.M. Silver [b,c], A. Gangopadhyay [b]

[a] Institute of Oceanography, University of São Paulo, Brazil
[b] Department of Estuarine and Ocean Sciences, School for Marine Science and Technology, University of Massachusetts Dartmouth, USA
[c] Woods Hole Oceanographic Institution, Woods Hole, MA 02543, USA

ARTICLE INFO

Keywords:
Phytoplankton blooms
Antarctic Polar Front
iron
Temperature effect

ABSTRACT

We demonstrate how the wind-driven Ekman transport enhances the advection and mixing of cells from the colder waters of the Surface Antarctic Waters from the south to the warmer waters of the northern Polar Front (PF) belt. This mechanism provides cells a mean ambient temperature near optimum levels for specific species and, ultimately, for community growth rates high enough to develop blooms under non-light limiting macronutrients and iron conditions. A Lagrangian trajectory model was constructed for tracking plankton cells as tracers forced by winds and surface currents. Depending on the region along the circumpolar front, increased winds can enhance this process across temperature gradients, and further accelerate such temperature-controlled growth. These results indicate that favorable temperature may enhance the growth rate even further when iron is sufficiently available, and thus have far-reaching implications for increased productivity in a future warming climate.

1. Introduction

The upper layers of the global ocean are commonly occupied by frontal systems with physical and/or biogeochemical gradients on a wide range of spatial scales (Longhurst, 2007; Belkin et al., 2009). They play an important role in pelagic ecosystem processes due to the exchange of biologically limiting properties between adjacent water masses and are sites of elevated primary productivity, biodiversity, and fisheries (Acha et al., *2015;* Woodson and Litvin, 2015). Oceanic fronts contribute towards the diagenesis of ocean floor sediments and ultimately to the carbon sink on a basin-wide scale (Longhurst, 2007; Ito et al., 2010). Particularly, along the Antarctic Circumpolar Current (ACC), the largest current of the global ocean, the polar frontal region plays a remarkable role in carbon sequestration (Smetacek et al., 1997; Ito et al., 2010 and references therein). The ACC carries large volumes of waters (*ca* 134 Sv) eastwards under the stress of westerly winds (Whitworth and Peterson, 1985; Orsi et al., 1995; Donohue et al., 2016).

The Subtropical Convergence (STC, 38-40^{0}S) and the Antarctic Convergence, also known as Antarctic Polar Front (hereafter PF, 50-65^{0}S), are the two most conspicuous oceanic fronts of the ACC, appearing in global climatological maps as hydrodynamic boundaries between subtropical, sub-Antarctic, and Antarctic water masses (Orsi et al., 1995; Moore et al., 1999; Dong et al., 2006; Graham and De Boer, 2013; Freeman and Lovenduski, 2016). Even minor changes in the capacity for atmospheric carbon sequestration at specific locations such as along fronts in such a large hydrographic domain will have major effects in the carbon cycling at the planetary scale (Ito et al., 2010). This is particularly true in the case of the PF because it is one of the most productive areas in the Southern Ocean, hence an important site of atmospheric CO_2 sequestration (Smetacek et al., 1997; Ito et al., 2010 and references therein) where temperature and biogeochemical gradients that enhance phytoplankton development might be affected by the expected global warming in the next decades (Christensen et al., 2007).

Diatoms usually dominate phytoplankton assemblages in oceanic fronts (Brandini et al., 2000; Smetacek et al., 1997; et al., 2002; DiTullio et al., 2003) making them important sites of atmospheric carbon uptake, hence contributing to the oceanic biological pump (Ito et al., 2010). Biogeochemical processes in the euphotic zone of wide and hydrographically homogeneous water masses are radically altered in frontal zones. The environmental properties that enhance phytoplankton growth may differ among fronts. For example, nutrients are the limiting factor in the STC, where heat exchange increases the euphotic zone stability and the input of macronutrients (mostly nitrate and silicate) from the nutrient-rich Sub-Antarctic region into the adjacent nutrient-

* Corresponding author.
E-mail addresses: brandini@usp.br (F.P. Brandini), asilver@umassd.edu (A.M. Silver), avijit.gangopadhyay@umassd.edu (A. Gangopadhyay).

https://doi.org/10.1016/j.jmarsys.2023.103909
Received 8 September 2022; Received in revised form 14 May 2023; Accepted 17 May 2023
Available online 19 May 2023

poor waters of the Subtropical Gyre (Brandini et al., 2000), turning this front into an ideal environment for the accumulation of diatoms (Brandini et al., 2000; Olguin et al., 2006). On the other hand, iron have been quoted as the main driver of phytoplankton growth on the PF (de Baar et al., 1995; Smetacek et al., 1997; Coale et al., 2003; Boyd et al., 2007; Tripathy and Jena, 2019), which represents the northern boundary of the Southern Ocean where cold surface waters to the south are separated from the warmer waters to the north (Moore et al., 1999; Belkin et al., 2009).

The location of the PF generally coincides with specific ranges of temperature and salinity (Park et al., 1998; Freeman and Lovenduski, 2016). In the uppermost layers of the front, Ekman-driven and geostrophic currents tend to move parcels from the colder Antarctic Surface Water near 2 °C from the south of the front towards the warmer (5–6 °C) northeast waters (Gnanadesikan and Hallberg, 2000; Freeman and Lovenduski, 2016). See more on the choice of the PF later in Section 2.2.

High chlorophyll concentrations of >0.5 mg m^{-3} and peak blooms of around 4 mg m^{-3} have been reported along the PF as compared to the range of 0.3–0.4 mg.m^{-3} reported in the sub-Antarctic zone to the north and in the colder surface waters of the ACC to the south (Bathmann et al., 1997; Smetacek et al., 1997; 2002). The hypothesis that iron is the main limiting factor for primary productivity in the High-Nutrient-Low-Chlorophyll (HNLC) regions of the Southern Ocean (Martin et al., 1990) has become a popular, if not the main, topic of Antarctic phytoplankton research for over two decades (de Baar et al., 1995; Coale et al., 2003; Boyd et al., 2007; Tripathy and Jena, 2019). Field and shipboard iron-enrichment experiments demonstrated the shift of the phytoplankton community composition towards larger macro-sized cells (mostly diatoms), and the increase of biomass and growth rate with the addition of iron (de Baar et al., 2005; Boyd et al., 2007; Tripathy and Jena, 2019). Hence, the positive effect of iron on the growth rates of phytoplankton has been proposed as the primary mechanism controlling phytoplankton blooms and atmospheric carbon uptake in the PF zone (de Baar et al., 1995; Coale et al., 2003).

However, our current understanding of the controls on phytoplankton growth and blooms in polar waters encompasses an interplay of multiple environmental drivers such as iron, light, nutrients and temperature (Neori and Holm-Hansen, 1982; Jacques, 1983; Fiala and Oriol, 1990; Mitchell et al., 1991; Andrew et al., 2019; Rose et al., 2009; Zhu et al., 2016). The question of which of these factors leads to the development of phytoplankton blooms at any given time and position still needs to be revisited, particularly along the PF where dissolved iron concentration is indeed exceptionally low (Klunder et al., 2014). For instance, it is worth noting that the PF blooms respond to iron-enrichment (de Baar et al., 2005; Boyd et al., 2007; Tripathy and Jena, 2019) where it coincides with the optimum temperatures for phytoplankton growth between 5 and 6 °C that have been often reported in the Antarctic literature (Neori and Holm-Hansen, 1982; Jacques, 1983; Fiala and Oriol, 1990; Coello-Camba and Agusti, 2017). This indicates the effect of in situ temperature should have been considered in the results of iron fertilization experiments in polar environments.

Here we hypothesize that, besides natural or artificial iron inputs, the rising temperature contributes towards increasing diatom growth rates during their Ekman-driven advection across the PF. To test this hypothesis, we first reconstruct a new region-specific growth-temperature regression model within the 0–6 °C temperature range, based on data available in the Antarctic literature (Table 1). We then carry out a robust set of clusters based Lagrangian simulations specific for the summer period (December, January and February) in the southern hemisphere, using circulation fields from a hydrodynamic model reanalysis across the PF zone in six longitudinal sectors (Moore et al., 1999; Table 2) of the Southern Ocean, representatives of the three different world ocean basins.

Table 1
Dataset of growth rates of Antarctic diatoms and natural communities growing under different temperature conditions used to develop the exponential temperature-growth rate Eq. (1).

Diatom species	T ^{0}C	k (d^{-1})	References
	2	0.33	Fiala and Oriol, 1990
	5	0.88	Fiala and Oriol, 1990
	5	1.05	Hoepffner, 1984
Chaetoceros deflandrei	5	1.02	Hoepffner, 1984
	3	0.41	Jacques, 1983
Chaetoceros sp.	5	0.63	Jacques, 1983
	3	0.33	Mortain-Bertrand, 1989
	0	0.13	Fiala and Oriol, 1990
Corethron criophilum	4	0.38	Fiala and Oriol, 1990
C. pennatum	4	0.25	Jacques, 1983
	3	0.25	Jacques, 1983
	5	0.48	Jacques, 1983
	0	0.3	Fiala and Oriol, 1990
	4	0.78	Fiala and Oriol, 1990
Fragilariopsis kerguelensis	4	0.52	Jacques, 1983
Navicula sp	4	0.34	Teoh et al., 2004
	0	0.27	Fiala and Oriol, 1990
Nitzschia cylindrus	5	0.86	Fiala and Oriol, 1990
	1	0.25	Fiala and Oriol, 1990
	3	0.71	Fiala and Oriol, 1990
	3	0.45	Jacques, 1983
	5	0.44	Jacques, 1983
	3	0.61	Mortain-Bertrand, 1989
	5	0.43	Hoepffner, 1984
Nitzschia turgiloides	5	0.39	Hoepffner, 1984
	1	0.42	Fiala and Oriol, 1990
	4	0.85	Fiala and Oriol, 1990
	3	0.13	Mortain-Bertrand, 1989
	3	0.18	Mortain-Bertrand, 1989
Stellarina microtrias	3	0.22	Mortain-Bertrand, 1989
	1	0.31	Fiala and Oriol, 1990
Synedra sp.	5	0.56	Fiala and Oriol, 1990
	4	0.6	Coello-Camba and Agusti, 2017
Thalassiosira sp.	4	0.45	Coello-Camba and Agusti, 2017
	2	0.54	Reay et al., 2001
	5	1.18	Reay et al., 2001
	4	0.4	Coello-Camba and Agusti, 2017
	5	0.82	Coello-Camba and Agusti, 2017
natural diatom community	5	0.82	Tilzer and Dubinsky, 1987

Table 2
Experimental domains selected within six different longitudinal sectors for carrying out representative simulations with varying degree of wind on these six different hydrographic/circulation regimes.

Region Name (Sectors)	Longitudinal Extent of Sectors	Latitudinal range of Polar Front	Initial Seed Location	Experimental Domain Identifier
Atlantic-Indian	50°W to 80°E	roughly 50°S	15°E, 50°S	A
Indian-Pacific	80°E to 160°E	50°-55°S	120°W, 55°S	B
Central Pacific	160°E to 170°W	60°-65°S	175°E, 60°S	C
Eastern Pacific	170°W to 130°W	55°-60°S	145°W, 56°S	D
Pacific-Atlantic	130°W to 70°W	60°-65°S	100°W, 60°S	E
Atlantic	70°W to 50°W	55°-60°S	60°W, 58°S	F

2. Materials and methods

2.1. Growth vs temperature regression model

We first constructed a growth rate vs temperature curve model (Fig. 1) specifically applicable for the Antarctic PF region where surface temperature usually ranges between 0 °C and 6 °C (Moore et al., 1999;

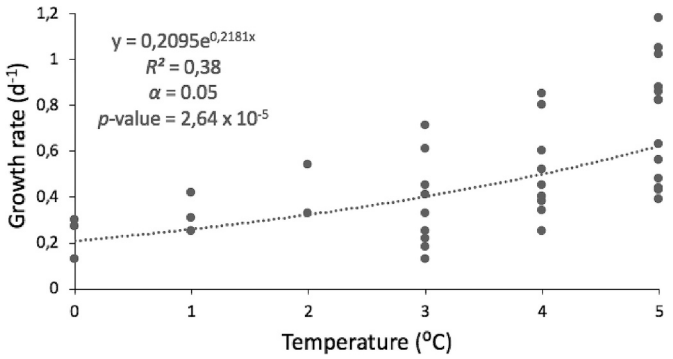

Fig. 1. Increasing pattern of specific growth rates of Antarctic diatoms and natural phytoplankton community as a function of temperature within the range of 0 to 5 °C. Dashed line represents the exponential regression fit between growth rate and temperature. The coefficient of determination R^2, significance level (α), and the null-hypothesis significance testing *(p-value)* were determined by the generalized linear model run by the R computing programing language.

Dong et al., 2006). The optimum temperature for the growth of most polar diatoms is *ca* 5 °C above which growth declines rapidly to lethal conditions (Jacques, 1983; Fiala and Oriol, 1990; Coello-Camba and Agusti, 2017; Boyd, 2019). Therefore, we only include in the growth rate (k) model temperatures up to 5 °C to avoid deviations of the positive relationship between growth rate and temperature. Our model is based on an empirical relationship of pairs of k vs T data points obtained from investigations where k of a specific diatom species has been measured at more than one temperature ranging from 0 to 5 °C. A total of 39 pairs of growth rates and temperature data were assembled (Table 1). Growth rates may be predicted from temperature by the exponential regression equation derived from the growth rate vs. temperature curve shown in Fig. 1.

$$k = 0.2095\ e^{0.2181T} \quad (1)$$

The goodness of fit, indicated as the coefficient of determination (R^2), and the statistical significance of the regression model (*p-value*) were quantified by the generalized linear model (GLM) run in the *R* statistical computing program. Eq. (1) was used later in the numerical model experiments for determining growth rates at various temperatures along the path of diatom cells while being advected by winds and circulation across the PF.

2.2. Numerical model experiments

A series of numerical experiments were carried out to assess the sensitivity of temperature-dependent growth in the presence of wind-induced advection across the front. The numerical experiments were based on Lagrangian tracking of seeded particles in a circulation field initialized from OSCAR (Ocean Surface Current Analysis Real-time) reanalysis at selected times (e.g., January 2016, or February 2019) and forced by pre-determined amplitudes of compatible wind forcing. This allows us to follow parcels from their initial seed locations, at the southern edge of the PF (approximated here as the 2 °C Sea Surface Temperature contour), as they are advected by the ocean surface currents and different levels of wind forcing, move from colder temperatures to warmer temperatures and help grow the plankton within the parcel.

To generate these different sensitivity simulations, data from two well-established gridded reanalysis fields were used. These are: (i) the ocean surface current reanalysis fields from OSCAR provided by the Earth and Space Research Institute at https://doi.org/10.5067/OSCAR-03D01; and (ii) the monthly surface temperature fields and mixed layer depths from the multi-observation global ocean 3-D ARMOR3D reanalysis. OSCAR combines a quasi-steady geostrophic model with wind driven ageostrophic and thermal wind adjustment components to obtain sea surface currents at a 1/3° resolution on a 5-day timescale (See white vectors Fig. 2). These weekly fields were then interpolated onto a daily timescale in order to avoid jumps within the flow fields. Monthly ARMOR3D (available through Copernicus Marine Services at https://data.marine.copernicus.eu/product/MULTIOBS_GLO_PHY_TSUV_3D_MYNRT_015_012/description) was used for its monthly sea surface temperature as well as the mixed layer depth which was used in the Ekman transport calculation. ARMOR3D combines satellites data with *in situ* temperature and salinity through statistical methods to give mixed layer depth and geostrophic currents fields at a 1/4° resolution (Mulet et al., 2012). In addition, 6-h reanalysis winds from JRA-55 (available from https://rda.ucar.edu/datasets/ds628.1/) were used to calculate the Ekman transport. We kept the winds at this 6-h time scale to account for the small-scale variability. Both the wind (6-hourly, 1.25° resolution) and ARMOR3D (monthly, 1/4° resolution) mixed layer depth data were interpolated on to the 1/3° resolution of the OSCAR fields for the 6-hourly advection simulation.

To investigate the role of wind driven forcing on diatoms across the PF a set of four numerical experiments were carried: (i) control, (ii) average wind; (iii) double-wind; and (iv) triple-wind (see Table 3). The control circulation field was derived by subtracting the wind-effects from the OSCAR circulation field to obtain a purely geostrophic flow. For the double wind and triple wind experiments the calculated Ekman transport was then added to OSCAR fields with appropriate weights. The average wind field just used the OSCAR data as is.

The calculation of wind driven Lagrangian trajectories can be explained in five steps. First the particle is dropped on the southern side of the PF. Wind velocity is then fed in at the given location and is used to calculate the wind stress (Gill, 1982; Large and Pond, 1981; Trenberth et al., 1990). Advective velocity due to Ekman drift is then calculated from this wind stress and the mixed layer depth (from ARMOR3D) based on a simple Ekman balance $V_{Ekman} = \frac{2M_y}{\rho H}$ (Gill, 1982). Here, V_{Ekman} is the surface velocity (assumed to decay linearly to zero at the base of mixed layer), M_y is the mass transport due to Ekman Drift and given by $M_y = \frac{\tau_x}{f}$, τ_x is the zonal wind stress in the longitudinal direction, f is the Coriolis parameter, ρ is the density of the water (1025 kg m^{-3}), and H is the mixed layer depth. Depending on the experiments these calculated Ekman velocities were then either added to (Expt # 3 and 4) or

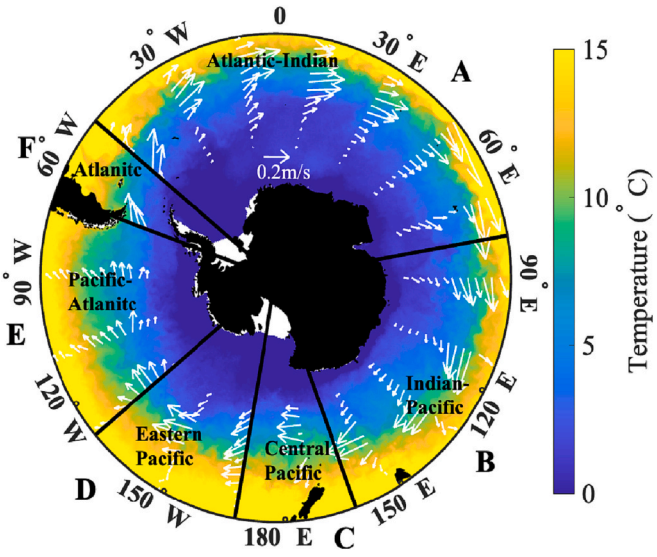

Fig. 2. Ocean circulation field (white velocity vectors) around the Antarctic (up to about 45°S) for January 2019 from OSCAR. Background color shows the sea surface temperature from ARMOR3d for January 2019. The six sectors based on Moore et al. (1999) study characterizes different variability of the Polar Front.

Table 3
Numerical Model Cluster Simulation Conditions with different wind forcing and OSCAR fields.

Experiment	Simulation condition	Data used for comparison
1	Control	OSCAR - Ekman
2	Average Wind	OSCAR
3	Double Wind	OSCAR + Ekman
4	Triple Wind	OSCAR +2*Ekman

subtracted from (Expt #1) the OSCAR velocities (Expt #2). The particle is then advected by this resulting velocity on the given trajectory for the one-hour time-step, after which the wind (from JRA-55), mixed layer depth (from ARMOR3D), and OSCAR velocities are reassessed at the new location in the given month. The Lagrangian tracking is then applied for another time-step (1 h) to yield a new advected location of the tracer (i.e., the phytoplankton cell). This continues for 28 days, a time interval necessary for a bloom development (Bathmann et al., 1997; Abbott et al., 2001; Landry et al., 2001) from a mean background ambient chlorophyll concentration of 0.2 mg m^{-3} in most of the Antarctic surface waters south of the PF zone at a mean chlorophyll accumulation rate of 0.027 d^{-1} (Barth et al., 2001; Landry et al., 2001). After each particle trajectory is run for the 28 day period, the temperature along the path is then interpolated from the monthly ARMOR3D SST field. We have used the monthly fields for temperature and mixed layer from ARMOR3D as opposed to the weekly fields because of two reasons. First, the usage of the monthly average temperature fields for extracting the temperature after advection should provide a conservative estimate of variability in temperature-derived growth rate compared to using weekly or daily fields. Second, due to its coarse sampling of the vertical water column, we used the monthly mixed layer depth from ARMOR3D as a conservative estimate to minimize error due to extrapolation in the reanalysis.

Particle seed locations were randomly selected in a ring around the 2 °C SST contour which were derived from the monthly ARMOR3D field with 1/4° spatial resolution. This was used here as an approximation for the southern edge of the PF. Seed locations were then randomly generated around this contour limited to being within a quarter of a degree latitude of the 2 °C line (Fig. 3). The PF thermal gradient is better defined at subsurface depths down to 200–300 m (Orsi et al., 1995; Belkin and Gordon, 1996; Park et al., 1998), i.e., further below euphotic layers which range from 40 to 80 m in open waters of ACC south of the PF (Ward et al., 2002); we choose to simulate the growth rate starting from the surface 2 °C contour. This is because the mean temperature of the Antarctic Surface Waters to the south of the Polar Front (Auger et al., 2021) is 2 °C, and captures the processes in the euphotic zone, (Gnanadesikan and Hallberg, 2000; Freeman and Lovenduski, 2016). In the upper euphotic layers light intensity saturates the photosynthetic rates and macronutrients are not limiting on both sides of the front (Brandini et al., 2000; DiTullio et al., 2003) to an extent that net production rates are fast enough to form the surface chlorophyll blooms observed along the PF (Bathmann et al., 1997; Smetacek et al., 1997; 2002). In other words, the model outputs would then be independent of a more uniform thermohaline gradient at deeper layers where light is not sufficient to account for bloom formation in the PF.

The total number of particles per run varied based on the length of the 2 °C contour for the given month with an average of 24,648 particles per month and a minimum of 22,980 particles which occurred in January 2014. This experiment was repeated for each of the 3 summer months (December, January and February) for 6 different years (December 2014 through January 2019). As seen in Fig. 3 B particles move both northward and southward. This is something that has been previously noted (Tamsitt et al., 2017). Fig. 3C shows a histogram of the change in temperature experienced by all particles in the average wind experiment for January 2019. In this histogram you can see both positive and negative ΔT with a slight skew towards positive end (Skewness = 0.84). This shows that particles move both north and south but move slightly more northward. Fig. 4 then shows the same information, ΔT for all particles in the average wind experiment for the month of January, but for all 6 years and divided into the different ocean basins. Here you can see that in all basins the mean ΔT (μ) is positive and in 4 out of the 6 basins the distribution is positively skewed. Table 4 then shows the μ and skewness values for average of three different months: December, January, and February. We have also run the experiments with weekly temperature and found the same trends between experiments with slightly larger ΔTs in all experiments. We present all results with the monthly simulations as they are more conservative and thus presents a lower bound of growth rate increase due to winds. For the purpose of looking at the effects of increased temperature, only particles with northward flow in the average wind experiments were selected. After each experiment was run the particles were divided into six longitudinal regions that were chosen based on Moore et al. (1999), with three domains bordering the Pacific basin, two domains bordering the Atlantic

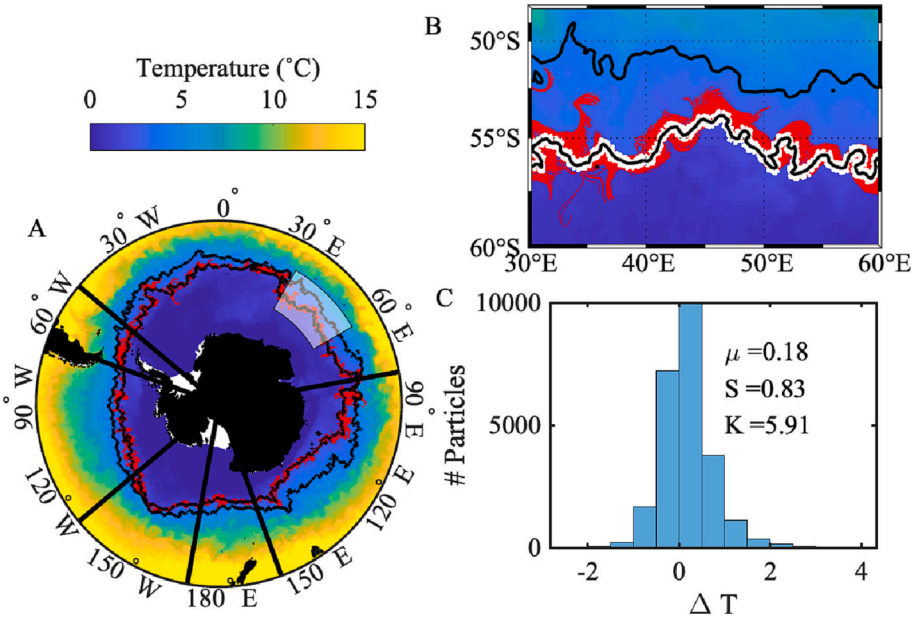

Fig. 3. Subplot A shows the sea surface temperature from January 2019 taken from ARMOR3D along with the approximate location of the 4 °C and 2 °C surface isotherms contours plotted in black representing the Polar Front. Thick black lines show the 6 geographical regions depicted in Fig. 2 and described in Table 2. Red lines show the individual particle paths for the average wind experiment during January 2019. Subplot B shows a zoomed in region of subplot A shown by the white shaded region. Again, the red lines are individual particle paths. The particle seeds were randomly located within the ¼° white band around the 2 °C contour line (in black). Note that these are approximate locations using a surface 2 °C isotherm to account for the euphotic zone being within the surface ~100 m. Subplot C shows a histogram of the change in sea surface temperature the individual particles experience from the start to the end of the 28 days for all particles in all six regions in January 2019. (For interpretation of the references to color in this figure legend, the reader is referred to the web version of this article)

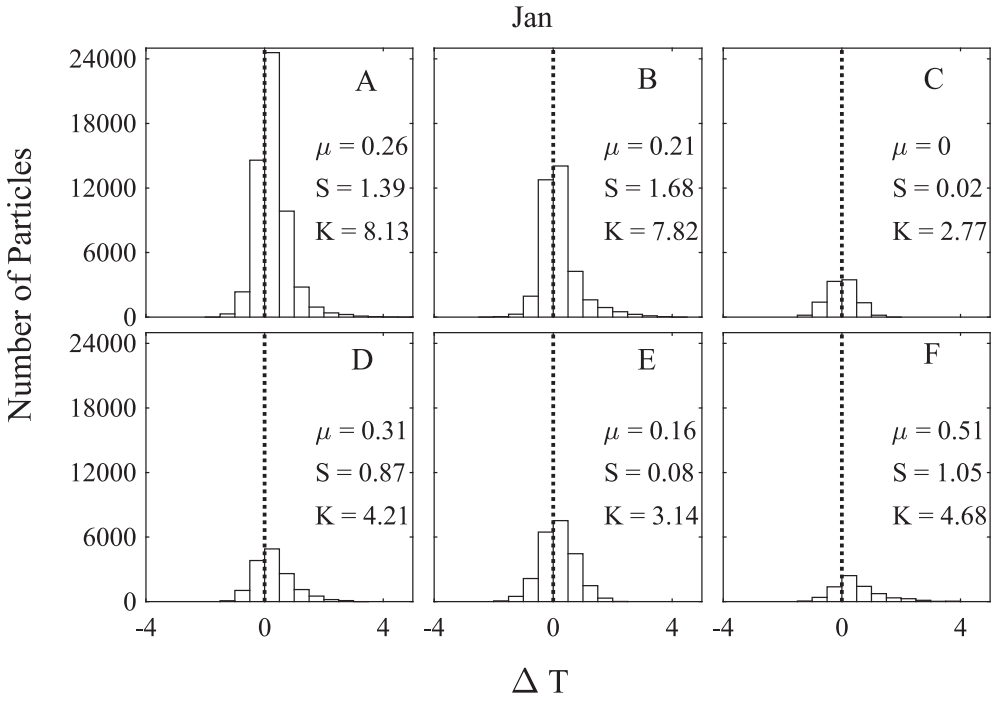

Fig. 4. Histograms showing the change in sea surface temperature following the particle trajectories for the average wind experiment for January of all six years divided in the 6 ocean basins. The average ΔT (μ), skewness (S) and kurtosis (K) of each histogram is shown in each subplot. The positive μ and s values both show that for all regions more particles travel to warmer water than to colder waters.

Table 4
The mean (μ), Skewness (S) and Kurtosis (K) values for the change in temperature from the start to the end times of northward particle advection on average in the 6 different Antarctic ocean basins for the average wind experiment for the months of December, January, and February. Most of the skewness are positive and most of the kurtosis values are >3, providing support for the northward particle advection to higher temperature and growth rates.

		A	B	C	D	E	F
Dec	Mu	0.41	0.31	0.11	0.41	0.24	0.94
	S	1.01	1.31	−0.20	0.48	0.05	0.08
	K	5.31	6.37	3.15	3.80	3.60	2.42
Jan	Mu	0.26	0.21	0.00	0.31	0.16	0.51
	S	1.39	1.68	0.02	0.87	0.08	1.05
	K	8.13	7.82	2.77	4.21	3.14	4.68
Feb	Mu	0.22	0.14	0.14	0.31	0.10	0.42
	S	1.46	0.89	0.37	1.54	0.16	0.08
	K	9.55	9.10	3.36	7.63	3.34	4.03

and one in the Indian basin (Table 2 and Fig. 2). The experimental section domains were selected based on the variability of the mean PF location in each region (Ito et al., 2010).

2.3. The model validation

Despite the limited data set, Eq. (1) reflects a consistent relationship between growth rate and temperature, and it was incorporated into a hydrodynamic model showing the potential northeastward transport of a particle representing a phytoplankton cell, along with a mass of colder water from the south limit of the PF (see Figs. 2 and 3 for the PF regional boundaries and temperature variation). The model uses Eq. (1) to calculate phytoplankton growth rates along with the gradient of rising temperature during their trajectory across the front in the 6 selected longitudinal sections (modeling domains in Fig. 3) of the Southern Ocean. These six regions are: going eastward starting from the Atlantic-Indian sector (Region A), Indian-Pacific sector (Region B), Central Pacific (Region C), Eastern Pacific (Region D), Pacific-Atlantic (Region E) and Atlantic (Region F). To investigate the role of wind driven forcing on diatoms across the PF in these 6 regions a set of four numerical experiments were carried out in each section: (i) control, (ii) average wind; (iii) double-wind; and (iv) triple-wind (Figs. 5, 6, and 7).

3. Results

The month-long trajectory simulations for each of the three months (December, January, and February) over six different years were averaged for the six different zones to generate a monthly average trajectory. Temperatures along the trajectory were then mapped to a corresponding growth rate using the new temperature-growth curve presented in Section 2.1, Fig. 1 and Eq. (1). This average growth rate progression for each region (A through F) for different wind-amplitude variations is presented in Figs. 5, 6 and 7 for December, January and February respectively. The shaded regions along each line then show the standard error from the mean (SEM) calculated from the 6-year average. Given that all particle seed locations were placed in water near 2 °C, the starting growth rate for each particle is around 0.32 d^{-1}. Once the particles begin to move northward into warmer waters the growth rate then increases as seen in Figs. 5-7. In regions where there is less northward movement, a more gradual increase in the growth rate is realized.

From these results we can see that there is large variation in the role of wind with varying longitudes, as well as months. For example, during the month of December (Fig. 5), it is evident that in regions A-C the northward movement of the particles seems to be more influenced by the wind than in regions D and E. This is seen by the triple (blue) and double (green) wind experiments having steeper slopes and reaching higher growth rates. In regions D and E, there is very little difference in the growth rates between the experiments indicating that wind might not play as strong of a role in these regions during December. Region F is unique in that the wind actually seems to push the particles southward with the control experiment showing the largest increase in growth rate.

There is also a difference in wind forcing between the different

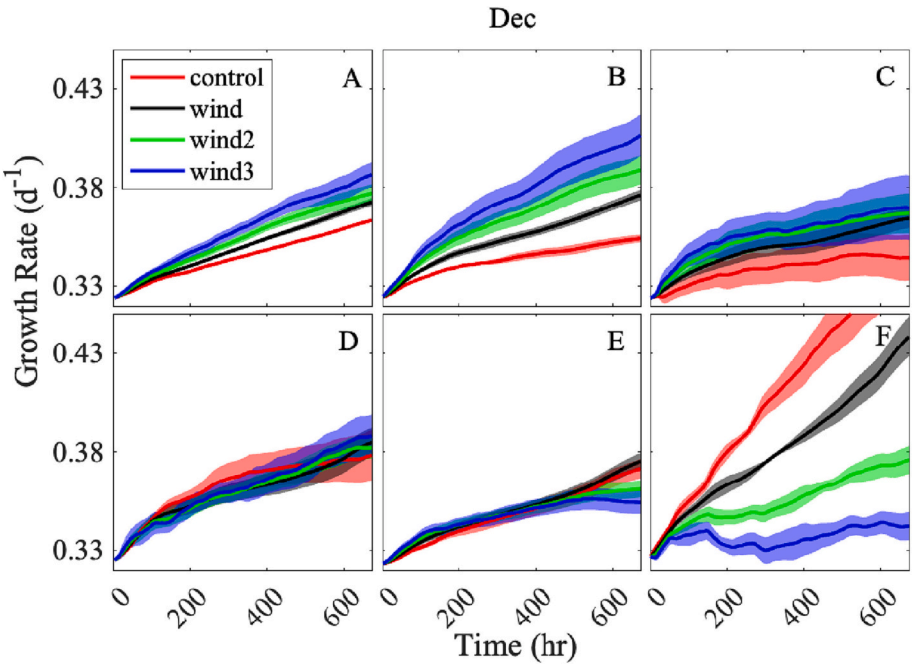

Fig. 5. Model simulated output showing changes in the Antarctic phytoplankton growth rate caused by changes in temperature in the six experimental sectors of the Polar Front for the month of December. See Table 1 and Fig. 2 for details of locations and regions. Solid lines represent the mean growth rate per day averaged over the 6-year period. The shaded region represents the mean ± SEM.

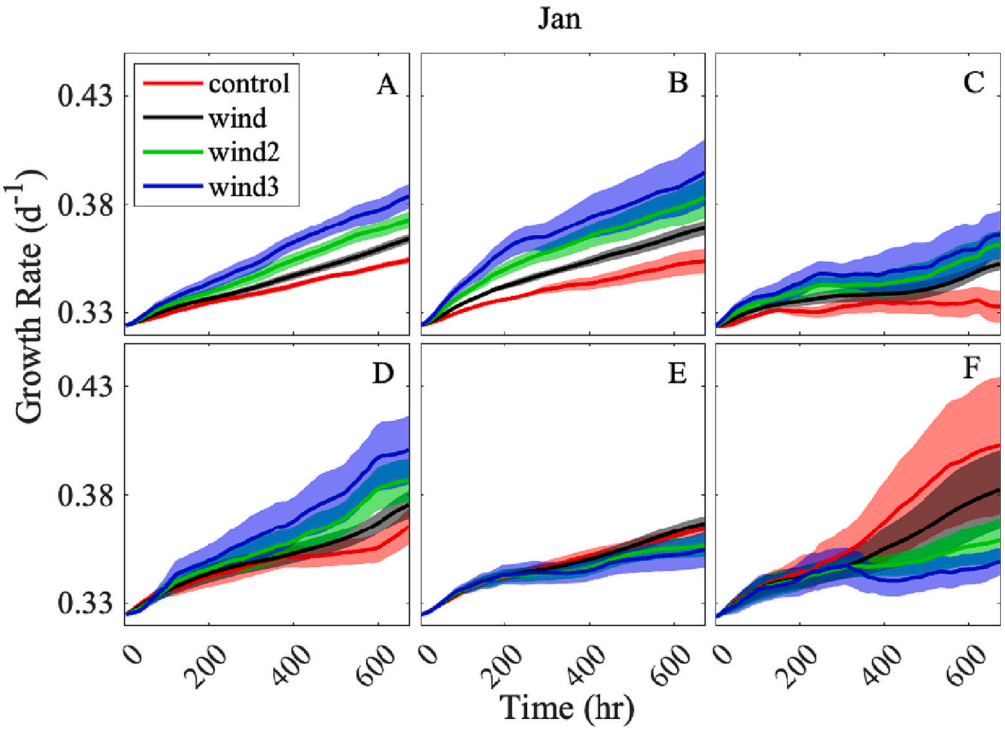

Fig. 6. Model simulated output showing changes in the Antarctic phytoplankton growth rate caused by changes in temperature in the six experimental sectors of the Polar Front for the month of January. See Table 1 and Fig. 2 for details of locations and regions. Solid lines represent the mean growth rate per day averaged over the 6-year period. The shaded region represents the mean ± SEM.

months. December and January seem to have the strongest wind forcing with the largest differences between experiments seen in these months. February shows very little difference between experiments of all regions indicating that winds might not play as large a role during this time.

4. Discussion

4.1. The growth-temperature regression model

The temperature vs growth rate model of Fig. 1 is consistent with the common observations of chlorophyll bloom development across the PF

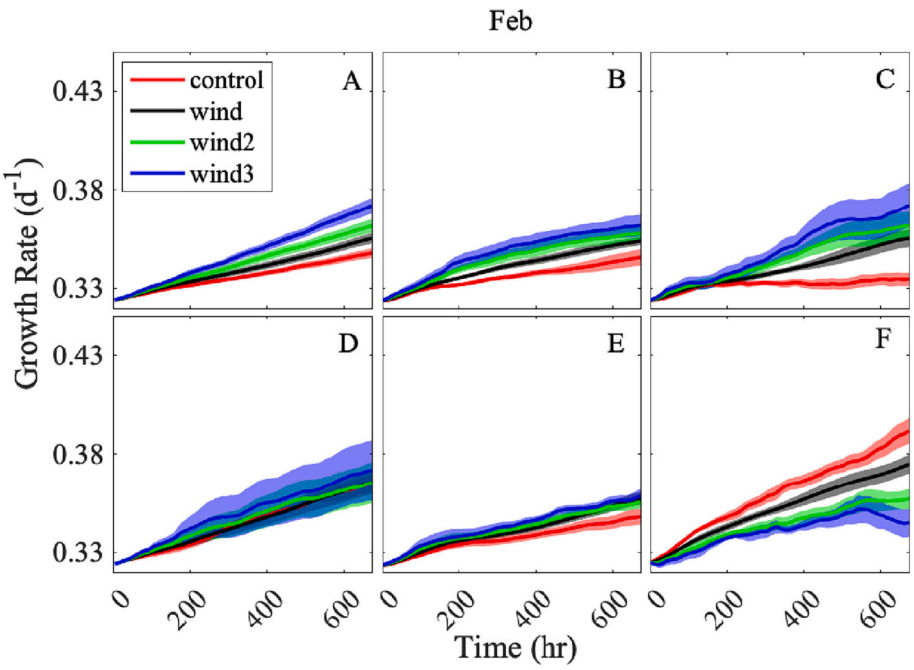

Fig. 7. Model simulated output showing changes in the Antarctic phytoplankton growth rate caused by changes in temperature in the six experimental sectors of the Polar Front for the month of February. See Table 1 and Fig. 2 for details of locations and regions. Solid lines represent the mean growth rate per day averaged over the 6-year period. The shaded region represents the mean ± SEM.

(Bathmann et al., 1997; Smetacek et al., 1997; et al., 2002). The circulation model's cluster simulation analysis suggests that the physical-biological interaction of exposing growing diatoms at near optimum ambient temperatures by the wind-driven advection process is an important, if not a primary driver for bloom development in the PF in the absence of iron. Earlier investigations suggested the Antarctic surface waters could be transported northwards together with diatom cells across the PF thermal gradient (Neori and Holm-Hansen, 1982), and the hydrodynamics of this transport has been later confirmed (Gnanadesikan and Hallberg, 2000). Our model demonstrates this might happen in all regions of the circumpolar PF belt.

Results from the numerical modeling sensitivity experiments can be summarized as follows. For all regions, increased winds increased the distance the particles traveled moving them into warmer waters and therefore increasing the growth rate. Some regions, particularly regions A, B, and C showed stronger influence of increased winds particularly in December and January. This can be seen by the increased difference in growth rates between experiments (Figs. 5 and 6). Region F in December (Atlantic sector) showed the largest northward transport when compared to the other regions with the strong northward flow being driven by the geostrophic transport with the wind being unfavorable in this region. Region F is unique in that the wind actually seems to push the particles southward with the control experiment showing the largest increase in growth rate. It is relevant to mention the role of eddies to explain this anomaly; In our model seed locations were selected to avoid eddies within the geostrophic flow field which are very prevalent within the PF and have the potential to prevent the particles northward movement. Hogg et al. (2015) reported the 40% increase of the surface westerly wind stress over the Southern Ocean over the past 40 years (*apud* Lin et al., 2018) affect more the number of eddies that transfer more heat poleward, particularly in specific places such as in the Drake Passage which is included in our F region. We have no data to confirm this argument, yet presumably the enhancement of eddy's frequency and strength could be a feasible explanation for the anomalous southward wind transport of the model particles in section F.

4.2. Linkages of the iron-induced Polar Front blooms to the physical and temperature-dependent growth rate

We reiterate the idea of the Polar Front blooms and their mechanistic linkages to the physical and temperature-dependent growth rate in the light of above results and discussion of simulations. Maximum growth rates of polar diatoms have been historically reported to occur above the ambient temperature (Neori and Holm-Hansen, 1982; Jacques, 1983; Fiala and Oriol, 1990), meaning the genetic evolution for temperature-dependent growth rate adaptation is still in progress in polar waters. Most shipboard iron-enrichment incubations and field fertilizations demonstrated changes in the phytoplankton composition towards larger macro-sized cells (mostly diatoms), enhanced physiological performance of the cells and the consequent increase of phytoplankton biomass (Timmermans et al., 2001; Coale et al., 2003; de Baar et al., 2005; Boyd, 2019). Despite that culture enrichments with iron usually give the expected community changes and biomass increase of diatoms, a more consistent growth rate trend of polar diatoms as a function of temperature and iron availability still needs to be achieved. It is worth noting that the sole addition or non-limitation of iron does not always double the growth rate of polar diatoms (Boyd, 2019). In contrast, temperature invariably increase growth rates when adjusted by only a few degrees above the ambient conditions (Jacques, 1983; Fiala and Oriol, 1990; Baumann et al., 1994; Boyd, 2019), and even in iron-limited conditions (Zhu et al., 2016; Andrew et al., 2019; Boyd, 2019).

The enhancement of polar diatom growth rates with increasing temperatures has been reported within the usual temperature range of the PF zone (Fiala and Oriol, 1990; Coello-Camba and Agusti, 2017; Andrew et al., 2019). Early investigations calculated up to a 50–100% increase of photosynthetic rates of natural Antarctic phytoplankton from ambient sub-zero temperatures up to 4–7 °C (Neori and Holm-Hansen, 1982; Jacques, 1983). Batch cultured diatoms collected in the Weddell Sea displayed a 200% increase of maxima growth rates when temperatures rose from −1.6 °C (ambient) to 1 °C (Baumann et al., 1994).

High chlorophyll concentrations up to 2 mg.m^{-3} under limiting iron conditions of 0.15–0.45 nM has been reported in the PF of the Atlantic sector justifying that past higher iron availability could have already

been incorporated by phytoplankton prior to their sampling survey (Smetacek et al., 2002). However, it is relevant to mention the potential effect of a temperature range of 1.2 °C reported in that article on biomass differences across the front. Our model predicts that under that temperature range growth rates could have been increased by 0.13 d^{-1}, which would be enough to double cell density in just five days. In addition, it has been reported Antarctic phytoplankton growth rates in coastal, presumably non-iron deficient, and offshore iron-limited waters tend to be similar if temperature is held constant (Banse, 1991). A difference of 40% between the growth rate of iron-replete and iron-deplete cultures was recently reported, yet the effect of temperature on the growth of both iron-deplete and iron-replete diatoms was remarkably higher (60–100%) (Andrew et al., 2019; Boyd, 2019) meaning the effect of temperature on the growth of polar diatoms can be higher than the isolated effect of iron. Past experiments conducted in the Ross Sea showed clear evidence about the importance of temperature in iron enriched diatom communities (Rose et al., 2009; Zhu et al., 2016). Rose et al. (2009) found highest final chlorophyll concentrations in deck-incubated bottles spiked with iron at higher temperatures (4 °C) than at 0 °C, and Zhu et al. (2016) reported a 61% increased growth rate of iron-depleted diatoms when both iron concentration and temperature where simultaneously increased.

Despite a seasonal decrease of *ca* 1 nM of iron stock over the upper 100 m layers across the PF region (de Baar et al., 1995), the left-over of 1–1.5 nM of iron was still above the minimum requirement of 0.2–1.0 nM of oceanic and coastal phytoplankton (Sunda et al., 1991; Brand, 1991) and within the range of the half-saturation constant (K_m) of 0.59–1.12 nM for iron uptake by polar diatoms (Timmermans et al., 2001) and at least 5× times higher than the K_m of 0.022 nM and 0.027 nM found in the northern and southern side of the PF, respectively (Coale et al., 2003). In addition, the necessity of iron for the synthesis of the enzyme nitrate reductase increases at lower temperatures (Timmermans et al., 2001), suggesting iron deficiency is alleviated in the warmer northern bound of the PF.

High concentrations of chlorophyll in cyclonic eddies formed in the front have been associated with cross-front transport of iron from the south to the north and heat from the north to the south (Kahru et al., 2007). The authors argued that heat exchange increases the physical stratification of the euphotic zone, reducing simultaneously iron and light limitations, hence favoring phytoplankton growth. Our model simulations suggest besides iron and non-light limited conditions, the higher mean temperature outside the eddy may be an additional driver for increasing phytoplankton growth rates and chlorophyll accumulation in the PF region.

5. Summary and conclusions

Environmental conditions for maximum phytoplankton growth and, eventually bloom formation, need the simultaneous interaction of multiple drivers (Tilzer and Dubinsky, 1987; Mortain-Bertrand, 1989; Reay et al., 2001; Longhi et al., 2003) to balance losses and increase net biomass. Yet for a bloom to develop in the PF growth rates must increase to a level that the ambient rising of temperature by itself may provide, independent or not of iron availability (Boyd, 2019).

Our model predicts the wind-driven Ekman transport and the mixing of cold south waters with the warm north waters of the front speed-up the iron-induced phytoplankton blooms in the PF. We demonstrate the wind field, combined with geostrophic flow in the PF zone, is an important driver exposing diatoms to optimal temperatures on the northern side of the front, enhancing their growth rates over that observed in the colder waters south of the front.

It is possible that stronger than usual winds might help decrease temperature in the northern part of the front, and thereby hinder the growth of phytoplankton. However, thermal gradients across the PF are very steady and are driven by the average wind field along the frontal zone. While anomalous wind stress may affect the thermal gradient at local scales, they do not persist long enough to affect this steadiness throughout the whole frontal system. That is the main reason why thermal gradients across the front are always there, and are well documented (Dong et al., 2006; Longhurst, 2007; Belkin et al., 2009).

Finally, our results do not contradict the fact that iron inputs may cause blooms development along the Southern Ocean, particularly along the PF where usual dissolved iron concentration is indeed exceptionally low (Klunder et al., 2014). Yet our model demonstrates the advection of cells across thermal gradients such as those found in the Polar Front cause temperature to act synergistically with iron for growth rate enhancement, suggesting the Southern Ocean may become one of the main sinks of atmospheric carbon if the increase in water temperature expected for the next decades (Christensen et al., 2007) is confirmed. The regression models of Figs. 5, 6, and 7 predict an approximate increase in growth rate from 0.3 up to 0.4 doublings day^{-1} in summer seasons only due to temperature increase, which corresponds to *ca* 25–30% more organic carbon production. This might explain the occurrences of chlorophyll blooms in the PF whenever the synergistic effect of iron and temperature concentration takes place. Anyway, predictions on this matter are still premature due to limited data set and the uncertainties about the future temperature scenarios in polar waters.

Funding

F.B. was supported by the grant no. 88881.313390/2019-01 from the Brazilian Ministry of Education and Culture.

Author contributions

F.P.B. conceived the research idea and wrote the manuscript with support from A.G. A.M.S. performed data calculations, worked with computer analyses, built up the model, and created the figures and tables. A.G. developed the model with support from A.S. and contributed to the discussion and analyses of the results.

Declaration of Competing Interest

The authors declare that they have no known competing financial interests or personal relationships that could have appeared to influence the work reported in this paper.

Data availability

Data will be made available on request.

Acknowledgements

We would like to acknowledge the support of SMAST and UMass Dartmouth for this study during the visit of FB from IOUSP (Brazil) to SMAST. The WindSat data used in our model was produced by Remote Sensing Systems and sponsored by the NASA Earth Science MEaSUREs DISCOVER Project and the NASA Earth Science Physical Oceanography Program. RSS WindSat data are available at www.remss.com. We thank two anonymous reviewers for their constructive critics and support to improve this article.

References

Abbott, M.R., Richman, J.G., Nahorniak, J.S., Barksdale, B.S., 2001. Meanders in the Antarctic Polar Frontal Zone and their impact on phytoplankton. Deep-Sea Res. II 48, 3891–3912. https://doi.org/10.1016/S0967-0645(01)00073-X.

Acha, E.M., Piola, A., Iribarne, O., Mianzan, H., 2015. Biology of fronts. In: Ecological Processes at Marine Fronts. Springer Briefs in Environmental Science. Springer, Cham. https://doi.org/10.1007/978-3-319-15479-4_3.

Andrew, S.M., Morell, H.T., Strzepek, R.F., Boyd, P.W., Ellwood, M.J., 2019. Iron availability influences the tolerance of Southern Ocean phytoplankton to warming and elevated irradiance. Front. Mar. Sci. 6 https://doi.org/10.3389/fmars.2019.00681 art681.

Auger, M., Morrow, R., Kestenare, E., Sallé, J.-B., Cowley, R., 2021. Southern Oean in situ temperature trends over 25 years emerge from interannual variability. Nat. Commun. 12, 514. https://doi.org/10.1038/s41467-020-20781-1.

Banse, K., 1991. Rates of phytoplankton cell division in the field and in iron enrichment experiments. Limnol. Oceanogr. 36, 1866–1898. https://doi.org/10.4319/lo.1991.36.8.1886.

Barth, J.A., Cowles, T.J., Pierce, S.D., 2001. Mesoscale physical and bio-optical structure of the Antarctic Polar Front near 170°W during austral spring. Geophys. Res. 106 https://doi.org/10.1029/1999JC000194, 13879–1390.

Bathmann, U.V., Scharek, R., Klass, C., Dubishar, C.D., Smetacek, V., 1997. Spring development of phytoplankton biomass and composition in major water masses of the Atlantic sector of the Southern Ocean. Deep-Sea Res. 44, 51–67. https://doi.org/10.1016/S0967-0645(96)00063-X.

Baumann, M.E.M., Brandini, F.P., Staubes, R., 1994. The influence of light and temperature on carbon specific DMS release by cultures of *Phaeocystis antarctica* and three Antarctic diatoms. Mar. Chem. 45, 129–136. https://doi.org/10.1016/0304-4203(94)90097-3.

Belkin, I.M., Gordon, A.L., 1996. Southern Ocean fronts from the Greenwich Meridian to Tasmania. J. Geophys. Res. 101, 3675–3696.

Belkin, I.M., Cornillon, P.C., Sherman, K., 2009. Fronts in large marine ecosystems. Prog. Oceanogr. 81, 223–236. https://doi.org/10.1016/j.pocean.2009.04.015.

Boyd, P.W., 2019. Physiology and iron modulate diverse responses of diatoms to a warming Southern Ocean. Nat. Clim. Chang. 9, 148–152. https://doi.org/10.1038/s41558-018-0389-1.

Boyd, P.W., Jickells, T., Laws, C.S., Blaine, S., Boyle, E.A., Buesseler, K.O., Coale, K.H., Cullen, J.J., De Baar, H.J.W., Follows, M., Harvey, M., Lancelot, C., Levasseur, M., Owens, N.P.J., Pollard, R., Rivkin, R.B., Sarmiento, J., Schoemann, V., Smetacek, V., Takeda, S., Tsuda, A., Turner, S., Watson, A.J., 2007. Mesoscale iron enrichment experiments 1993–2005: synthesis and future directions. Science 315, 612–617. https://doi.org/10.1126/science.1131669.

Brand, L.E., 1991. Minimum iron requirements of marine phytoplankton and the implications for the biogeochemical control of new production. Limnol. Oceanogr. 36, 1756–1771. https://doi.org/10.4319/lo.1991.36.8.1756.

Brandini, F.P., Boltovskoy, D., Piola, A., Kocmur, S., Röttgers, R., Abreu, P.C., Lopes, R. M., 2000. Multiannual trends in fronts and distribution of nutrients and chlorophyll in the southwestern Atlantic (30-62°S). Deep-Sea Res. I 47, 1015–1033. https://doi.org/10.1016/S0967-0637(99)00075-8.

Christensen, J.H., Hewitson, B., Busuioc, A., Chen, A., Gao, X., Held, I., et al., 2007. Regional climate projections. In: Solomon, S., Qin, D., Manning, M., Chen, Z., Marquis, M., Averyt, K.B., Tignor, M., Miller, H.L. (Eds.), IPCC Climate Change 2007: The Physical Science Basis. Cambridge University Press, Cambridge, UK; New York, NY, pp. 849–940.

Coale, K.H., Wang, X., Tanner, S.J., Johnson, K.S., 2003. Phytoplankton growth and biological response to iron and zinc addition in the Ross Sea and Antarctic Circumpolar Current along 170°W. Deep-Sea Res. 50, 635–653. https://doi.org/10.1016/S0967-0645(02)00588-X.

Coello-Camba, A., Agusti, S., 2017. Thermal thresholds of phytoplankton growth in polar waters and their consequences for a warming Polar Ocean. Front. Mar. Sci. 4 https://doi.org/10.3389/fmars.2017.00168 ra168.

de Baar, H.J.W., de Jong, J.T.M., Bakker, D.C.E., Löscher, B.M., Veth, C., Bathmann, U., Smetacek, V., 1995. Importance of iron for plankton blooms and carbon dioxide drawdown in the Southern Ocean. Nature 373, 412–415. https://doi.org/10.1038/373412a0.

de Baar, H.J.W., Boyd, P.H., Coale, K.H., et al., 2005. Synthesis of iron fertilization experiments: from the iron age in the age of enlightenment. J. Geophys. Res. 110 https://doi.org/10.1029/2004JC002601. C09S16.

DiTullio, G.R., Geesey, M.E., Jones, D.R., Daly, K.L., Campbell, L., Smith Jr., W.O., 2003. Phytoplankton assemblage structure and primary productivity along 170 W in the South Pacific Ocean. Mar. Ecol. Prog. Ser. 255, 55–80. https://doi.org/10.3354/meps255055.

Dong, S., Sprintfall, J., Gill, S.T., 2006. Location of the Antarctic Polar Front from AMSR-E satellite sea surface temperature measurements. J. Phys. Oceanogr. 36, 2075–2089 (http://113.160.249.209:8080/xmlui/handle/123456789/9061).

Donohue, K.A., Tracey, K.L., Watts, D.R., Chidichimo, M.P., Chereskin, T.K., 2016. Mean Antarctic circumpolar current transport measured in Drake Passage. Geophys. Res. Lett. 43, 11760–11767. https://doi.org/10.1002/2016GL070319.

Fiala, M., Oriol, M.L., 1990. Light-temperature interactions on the growth of Antarctic diatoms. Polar Biol. 10, 629–636. https://doi.org/10.1007/BF00239374.

Freeman, N.M., Lovenduski, N.S., 2016. Mapping the Antarctic Polar Front: weekly realizations from 2002 to 2014. Earth Syst. Sci. Data 8, 191–198. https://doi.org/10.5194/essd-8-191-2016.

Gill, A.E., 1982. Atmosphere-Ocean Dynamics, vol. 30. Academic Press, New York, p. 662p.

Gnanadesikan, A., Hallberg, R.W., 2000. On the relationship of the circumpolar current to southern hemisphere winds in coarse-resolution ocean models. J. Phys. Oceanogr. 30, 2013–2034. https://doi.org/10.1175/15200485(2000)030<2013:OTROTC>2.0.CO;2.

Graham, R.M., De Boer, A.M., 2013. The dynamical subtropical front. J. Geophys. Res. 118, 5676–5685. https://doi.org/10.1002/jgrc.20407.

Hoepffner, N., 1984. Stratégies d'adaptation photosynthétique chez les diatomées de l'Océan Antarctique: variations du nombre et de la taille des units photosynthétiques. J. Plankton Res. 6, 881–895. https://doi.org/10.1093/plankt/6.5.881.

Hogg, A.M., Meredith, M.P., Chambers, D.P., Abrahamsen, E.P., Hughes, C.W., Morrison, A.K., 2015. Recent trends in the Southern Ocean eddy field. J. Geophys. Res. 120, 257–267. https://doi.org/10.1002/2014JC010470.

Ito, T., Woloszyn, M., Mazloff, M., 2010. Anthropogenic carbon dioxide transport in the Southern Ocean driven by Ekman flow. Nat. Lett. 463 https://doi.org/10.1038/nature08687.

Jacques, G., 1983. Some Ecophysiological aspects of the Antarctic phytoplankton. Polar Biol. 2, 27–33. https://doi.org/10.1007/BF00258282.

Kahru, M., Mitchell, B.G., Gille, S.T., Hewes, C.D., Holm-Hansen, O., 2007. Eddies enhance biological production in the Weddell-scotia confluence of the Southern Ocean. Geophys. Res. Lett. 34 https://doi.org/10.1029/2007GL030430. LI 14603.

Klunder, M.B., Laan, P., de Baar, H.J.W., Middag, R., Neven, I., van Oiijen, J., 2014. Dissolved Fe across the Weddell Sea and Drake Passage: impact of DFe on nutrient uptake. Biogeosciences 11, 651–669. https://doi.org/10.5194/bg-11-651-2014.

Landry, M.R., Brown, S.L., Selph, K.E., Abbot, M.R., Letelier, R.M., Christensen, S., Bidigare, R.R., Casciotti, K., 2001. Initiation of the spring phytoplankton increase in the Antarctic Polar Front Zone at 170°W. J. Geophys. Res. 106, 13903–13915. https://doi.org/10.1029/1999JC000187.

Large, W.G., Pond, S., 1981. Open Ocean momentum flux measurements in moderate to strong winds. J. Phys. Oceanogr. 11, 324–336.

Lin, X., Zhai, X., Wang, Z., Munday, D.R., 2018. Mean, variability, and trend of Southern Ocean wind stress: role of wind fluctuations. 2018. J. Clim. 31, 3557–3573. https://journals.ametsoc.org/view/journals/clim/31/9/jcli-d-17-0481.1.xml.

Longhi, M.L., Schloss, I.R., Wiencke, C., 2003. Effect of irradiance and temperature on photosynthesis and growth of two Antarctic benthic diatoms, *Gyrosigma subsalinum* and *Odontella litigiosa*. Bot. Mar. 46, 276–284. https://doi.org/10.1515/BOT.2003.025.

Longhurst, A.R., 2007. Ecological Geography of the Sea, 2nd ed. Academic Press, San Diego. https://doi.org/10.1016/B978-0-12-455521-1.X5000–1. 542p.

Martin, J.H., Fitzwater, S.E., Gordon, R.M., 1990. Iron deficiency limits phytoplankton growth in Antarctic waters. Glob. Biogeochem. Cycles 4, 5–12. https://doi.org/10.1029/GB004i001p00005.

Mitchell, B.G., Brody, E.A., Holm-Hansen, O., McClain, C., Bishop, J., 1991. Light limitation of phytoplankton biomass and macronutrient utilization in the Southern Ocean. Limnol. Oceanogr. 36, 1662–1677. https://doi.org/10.4319/lo.1991.36.8.1662.

Moore, J.K., Abbott, M.R., Richman, J.G., Smith, W.O., Cowles, T.J., Coale, K.H., Gardner, W.D., Barber, R.T., 1999. SeaWiFS satellite ocean color data from the Southern Ocean. Geophys. Res. Lett. 26, 1465–1468. https://doi.org/10.1029/1999GL900242.

Mortain-Bertrand, A., 1989. Effects of light fluctuations on growth and productivity of Antarctic diatoms in culture. Polar Biol. 9, 245–252. https://doi.org/10.1007/BF00263772.

Mulet, S., Rio, M.H., Mignot, A., Guinehut, S., Morrow, R., 2012. A new estimate of the global 3D geostrophic ocean circulation based on satellite data and in-situ measurements. Deep-Sea Res. II Top. Stud. Oceanogr. 77–80, 70–81. https://doi.org/10.1016/j.dsr2.2012.04.012.

Neori, A., Holm-Hansen, O., 1982. Effect of temperature on rate of photosynthesis in Antarctic phytoplankton. Polar Biol. 1, 33–38. https://doi.org/10.1007/BF00568752.

Olguin, H.F., Boltovskoy, D., Lange, C.D., Brandini, F.P., 2006. Distribution of spring phytoplankton (manly diatom) in the upper 50 m of the Southwestern Atlantic Ocean (30-60°S). J. Plankton Res. 28, 1107–1128. https://doi.org/10.1093/plankt/fb1045.

Orsi, A.H., Whitworth, T., Nowling Jr., W.D., 1995. On the meridional extent and fronts of the Antarctic Circumpolar Current. Deep-Sea Res. I Oceanogr. Res. Pap. 42 (5), 641–673. https://doi.org/10.1016/0967-0637(95)00021-W.

Park, Y.-H., Charriaud, E., Fieux, M., 1998. Thermohaline structure of the Antarctic surface water/winter water in the Indian sector of the Southern Ocean. J. Mar. Syst. 17 (1–4), 5–23. https://doi.org/10.1016/S0924-7963(98)00026-8.

Reay, D., Priddle, J., Nedwell, D.B., Whitehouse, M.J., Ellis-Evans, J.C., Deubert, C., Connelly, D.P., 2001. Regulation by low temperature of phytoplankton growth and nutrient uptake in the Southern Ocean. Mar. Ecol. Prog. Ser. 219, 51–64. https://doi.org/10.3354/meps219051.

Rose, J.M., Feng, Y., DiTullio, G.R., Dunbar, R.B., Hare, C.E., Lee, P.A., Lohan, M., Long, M., Smith Jr., W.O., Sohst, B., Tozzi, S., Zhang, Y., Hutchins, D.A., 2009. Synergistic effects of iron and temperature on Antarctic plankton assemblages. Biogeosci. Discuss. 6, 5849–5889. https://doi.org/10.5194/bgd-6-5849-2009.

Smetacek, V., de Baar, H.J.W., Bathmann, U.V., Lochte, K., van der Loeff, R., 1997. Ecology and biogeochemistry of the Antarctic Circumpolar Current during austral spring: a summary of Southern Ocean JGOFS cruise ANT X/6 of R.V. Polarstern. Deep-Sea Res. II 44, 1–21. https://epic.awi.de/id/eprint/2940/.

Smetacek, V., Klaas, C., Mewnde-Deuer, S., Rynearson, T.A., 2002. Mesoscale distribution of dominant diatom species relative to hydrographical field along the Antarctic Polar Front. Deep-Sea Res. II 49, 3835–3848. https://doi.org/10.1016/S0967-0645(02)00113-3.

Sunda, W.G., Swift, D.G., Huntsman, A.S., 1991. Low iron requirement for growth in oceanic phytoplankton. Nature 351, 55–57. https://doi.org/10.1038/351055a0.

Tamsitt, V., Drake, H.F., Morrison, A.K., et al., 2017. Spiraling pathways of global deep waters to the surface of the Southern Ocean. Nat. Commun. 8, 172. https://doi.org/10.1038/s41467-017-00197-0.

Teoh, M.L., Chu, W.L., Marchant, H., Phang, S.M., 2004. Influence of culture temperature on the growth, biochemical composition and fatty acid profiles of six Antarctic microalgae. J. Appl. Phycol. 16, 421–430. https://doi.org/10.1007/s10811-004-5502-3.

Tilzer, M.M., Dubinsky, Z., 1987. Effects of temperature and day length on the mass balance of Antarctic phytoplankton. Polar Biol. 7, 35–42. https://doi.org/10.1007/BF00286822.

Timmermans, K.R., Gerringa, L.J.A., de Baar, H.J.W., van der Wagt, B., Veldhuis, M.J.W., de Jong, J.T.M., Croot, P.L., 2001. Growth rates of large and small Southern Ocean diatoms in relation to availability of iron in natural seawater. Limnol. Oceanogr. 46, 260–266. https://doi.org/10.4319/lo.2001.46.2.0260.

Trenberth, K.E., Large, W.G., Olson, J.G., 1990. The mean annual cycle in global ocean wind stress. J. Phys. Oceanogr. 20, 1742–1760.

Tripathy, S.C., Jena, B., 2019. Iron-stimulated phytoplankton blooms in the Southern Ocean: a brief review. Remote Sens. Earth Syst. Sci. 2, 64–77. https://doi.org/10.1007/s41976-019-00012-y.

Ward, P., Whitehouse, M., Meredith, M., Murphy, E., Shreeve, R., Korb, R., Watkins, J., Thorpe, S., Woodd-Walker, R., Brierley, A., Cunningham, N., Grant, S., Bone, D., 2002. The Southern Antarctic Circumpolar Current Front: physical and biological coupling at South Georgia. Deep-Sea Res. I Oceanogr. Res. Pap. 49 (12), 2183–2202. https://doi.org/10.1016/S0967-0637(02)00119-X.

Whitworth, T., Peterson, R.G., 1985. Volume transport of the Antarctic Circumpolar Current from bottom pressure measurements. J. Phys. Oceanogr. 15, 810–816.

Woodson, C.B., Litvin, S.Y., 2015. Ocean fronts drive marine fishery production and biogeochemical cycling. Proc. Natl. Acad. Sci. U. S. A. 112, 1710–1715. https://doi.org/10.1073/pnas.141714311.

Zhu, Z., Kai Xu, K., Fu, F., Spackeen, J.L., Bronk, D.A., Hutchins, D.A., 2016. A comparative study of iron and temperature interactive effects on diatoms and Phaeocystis antarctica from the Ross Sea, Antarctica. Mar. Ecol. Prog. Ser. 550, 39–51. https://doi.org/10.3354/meps11732.